Soils and Foundations 2013;53(5):639–652

The Japanese Geotechnical Society

Soils and Foundations

www.sciencedirect.com
journal homepage: www.elsevier.com/locate/sandf

Active static and seismic earth pressure for c–φ soils

Magued Iskander*, Zhibo (Chris) Chen , Mehdi Omidvar, Ivan Guzman, Omar Elsherif

Polytechnic Institute of New York University, USA

Received 1 October 2012; received in revised form 23 April 2013; accepted 15 June 2013
Available online 26 September 2013

Abstract

Rankine classic earth pressure solution has been expanded to predict the seismic active earth pressure behind rigid walls supporting c–φ backfill considering both wall inclination and backfill slope. The proposed formulation is based on Rankine's conjugate stress concept, without employing any additional assumptions. The developed expressions can be used for the static and pseudo-static seismic analyses of c–φ backfill. The results based on the proposed formulations are found to be identical to those computed with the Mononobe–Okabe method for cohesionless soils, provided the same wall friction angle is employed. For c–φ soils, the formulation yields comparable results to available solutions for cases where a comparison is feasible. Design charts are presented for calculating the net active horizontal thrust behind a rigid wall for a variety of horizontal pseudo-static accelerations, values of cohesion, soil internal friction angles, wall inclinations, and backfill slope combinations. The effects of the vertical pseudo-static acceleration on the active earth pressure and the depth of tension cracks have also been explored. In addition, examples are provided to illustrate the application of the proposed method.
© 2013 The Japanese Geotechnical Society. Production and hosting by Elsevier B.V. All rights reserved.

Keywords: Mononabe–Okabe method; Rankine; Retaining wall; Seismic; Limit state analysis

1. Introduction

The estimation of seismic active earth pressure on retaining walls from backfill soils is an important problem in earthquake engineering. Pioneering works on seismic earth pressure on a rigid retaining wall have been reported by Okabe (1924) and Mononobe and Matsuo (1929, 1932). Their analyses have provided a popular solution to the problem of cohesionless soils. The Mononobe–Okabe (M–O) method is a pseudo-static approach, which incorporates seismic accelerations in the form of inertial forces into Coulomb's 1776 limit equilibrium analysis (Heyman, 1997). While the original M–O solution did not account for cohesion, several authors have extended the M–O solution to account for c–φ soils. For example, Saran and Prakash (1968) and Saran and Gupta (2003) proposed a solution for seismic earth pressure on a retaining wall supporting c–φ soils, in which the contributions of soil weight and cohesion are optimized separately, in some cases leading to two distinct failure planes. Shukla et al. (2009) developed an expression for the total seismic active force on a retaining wall supporting c–φ backfill based on the Coulomb sliding wedge concept, disregarding the soil–wall friction component. In all Coulomb type of solutions, only force equilibrium is used; and therefore, the distribution of the lateral thrust is not determined. On the other hand, Rankine's (1857) active earth pressure is a stress field-based solution, which does not require specifying failure kinematics (Huntington, 1957). The original Rankine solution considered static lateral earth pressure against

*Corresponding author.
E-mail address: Iskander@poly.edu (M. Iskander).
Peer review under responsibility of The Japanese Geotechnical Society.

Production and hosting by Elsevier

0038-0806 © 2013 The Japanese Geotechnical Society. Production and hosting by Elsevier B.V. All rights reserved.
http://dx.doi.org/10.1016/j.sandf.2013.08.003

a vertical rigid wall supporting cohesionless backfill with a ground surface unlimited in lateral extent and depth. Chu (1991) extended Rankine's method to account for wall inclination, and Mazindrani and Ganjali (1997) presented a similar solution for cohesive backfill under static conditions. Limitations of stress-based solutions, as well as a discussion on the general limitations of Coulomb-type solutions can be found in Mylonakis et al. (2007).

In addition to Coulomb and Rankine's earth pressure theory, other theoretical solutions have been developed to compute lateral earth pressure. Caquot and Kerisel (1948) developed tables of earth pressure coefficients based on the logarithmic spiral failure surface. Sokolovskii (1965) developed a characteristic method to compute lateral earth pressure based on a finite-difference solution. Habibagahi and Ghahramani (1979) developed a solution for lateral earth pressure coefficients based on the zero extension line theory. Notwithstanding the significance of these contributions, none of the aforementioned methods can be used for c–φ backfill under seismic conditions. Richards and Shi (1994) presented a plasticity-based solution to calculate seismic lateral earth pressure limited to vertical walls retaining horizontal c–φ backfill. Due to the complexity of the soil–wall interaction, numerical techniques have recently been adopted to compute the seismic earth pressure against a retaining wall (Al-Homoud and Whitman, 1994; Gazetas et al., 2004; Psarropoulos et al., 2005; Madabhushi and Zeng, 2007; Tiznado and Rodriguez-Roa, 2011). However, numerical modeling is generally costly, time consuming and difficult to implement.

In practice, when computing earth pressure against retaining walls, it is often assumed that the backfill is cohesionless. However, most natural deposits have some fines content that exhibits some degree of cohesion (Sitar et al., 2012). Anderson et al. (2008) found that the contribution of cohesion to a reduction in seismic earth pressure on retaining walls could be in the order of approximately 50%. Lew et al. (2010a, 2010b) compared the seismic performance of various retaining structures in recent earthquakes and reached a similar conclusion. Therefore, it is worthwhile to consider the cohesion in backfill for retaining structure problems. As pointed out by Sitar et al. (2012), "*the costs of an overconservative design can be just as much of a problem as the cost of a future failure*". Other factors, including the generation of negative pore air pressure in backfills during earthquakes (Koseki et al., 2010) and the outward movement of a retaining wall under large seismic loads (Watanabe et al., 2011), may also reduce the seismic active earth pressure.

In this paper, Rankine's conjugate stress approach for pseudo-static active earth pressure behind inclined rigid walls supporting sloped backfill, proposed by Iskander et al. (2012), has been generalized for cohesive backfill. The validity of the solution is demonstrated through a comparison with the available solutions to the problem.

2. Analytical formulation

The original Rankine active earth pressure solution assumes that the soil behind a retaining wall follows the movement of the wall, and the whole soil mass is subjected to uniform lateral extension. This implies that a uniform stress field exists and that the stress field of the soil behind the wall will be equal to that in the free field. This assumption is generally not true, since the stress in the near field behind the wall is different from that in the free field due to the difference in the movement between the wall and the free field (Richards et al., 1999) and the effects of soil arching (Paik and Salgado, 2003). However, following Rankine's original assumptions, we assume in this paper that the stress field adjacent to the wall is the same as that in the free field, disregarding the errors associated with such an assumption.

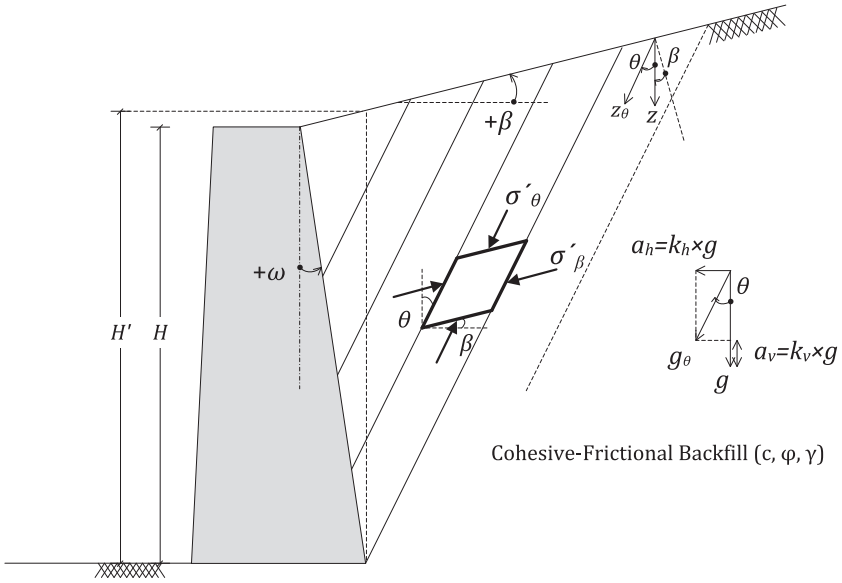

Fig. 1. Problem geometry and conjugate stress state in soil element behind backfill.

The pseudo-static method is adopted in our formulation to analyze the seismic response of backfill on the retaining wall, which ignores the time effect of the applied earthquake load. As a result, it cannot represent the actual complex seismic behavior of the soil during an earthquake (Nakamura, 2006; Ghosh and Sharma, 2010). Nevertheless, it is still one of the most popular approaches used in earthquake engineering. In the pseudo-static approach, seismic forces are represented as inertial body forces acting on the wall, in addition to other static forces. These seismic forces are computed using uniform pseudo-static horizontal and vertical accelerations, $a_h=k_hg$ and $a_v=k_vg$, where k_h and k_v are the horizontal and vertical seismic coefficients, respectively.

Consider the problem shown in Fig. 1, namely, a rigid, inclined wall with an inclination of ω retaining a c–φ backfill of surface slope β and unit weight γ, internal friction angle φ and cohesion c. The combined action of gravitational acceleration, g, and the horizontal and vertical pseudo-static accelerations, a_h and a_v, can be represented by a single acceleration field acting at an angle θ to the vertical, as denoted in Fig. 1 (Lancellotta, 2007). Therefore, the effect of the inertial forces can be incorporated into the static problem by modifying the acceleration field to a modified value of g_θ, oriented at an angle θ to the vertical. It then follows that γ is also modified to γ_θ. Modified acceleration field g_θ has a modified unit weight γ_θ and is inclined to the vertical axis by an angle θ, which are obtained as follows:

$$g_\theta = \sqrt{(g \pm a_v)^2 + a_h^2} \tag{1}$$

$$\theta = \tan^{-1}\left(\frac{a_h}{g \pm a_v}\right) = \tan^{-1}\left(\frac{k_h}{1 \pm k_v}\right) \tag{2}$$

$$\gamma_\theta = \frac{\gamma}{\cos\,\theta}(1 \pm k_v) \tag{3}$$

It should be noted that the positive sign applies for the downward direction and the negative sign applies for the upward direction of the vertical seismic force. The overburden pressure, at any given depth z below the sloping ground surface, can be calculated along angle θ on a modified axis referred to as z_θ. Modified effective stress σ_θ', that includes the inertial effects (Fig. 1), can be calculated using the following relation:

$$\sigma_\theta' = \gamma_\theta z_\theta \cos(\theta+\beta) = \left(\frac{\gamma}{\cos\,\theta}(1 \pm k_v)\right) \times \left(\frac{z\,\cos\,\beta\,\cos(\beta+\theta)}{\cos(\beta+\theta)}\right) = \gamma z(1 \pm k_v)\frac{\cos\,\beta}{\cos\,\theta} \tag{4}$$

Rankine (1858) states, "*if the stress on a given plane in a body be in a given direction, the stress on any plane parallel to that direction must be in a direction parallel to the first mentioned plane*". A soil element, at a vertical depth z below the sloping ground surface in free field conditions, corresponding to the problem under consideration, is depicted in Fig. 2 with the four corners labeled as a, b, c and d. Planes bc and ad are chosen to be oriented parallel to the ground surface, while planes ab and cd are oriented at an angle θ to the vertical, where θ has been defined by Eq. (2). The modified effective stress acts σ_θ' on planes bc and ad, which are parallel. Therefore, according to the conjugate stress principle, the stress acting on planes ab and cd (which are parallel to the plane of σ_θ') is parallel to plane bc. Stress planes bc and cd are termed conjugate planes, and corresponding stresses σ_θ' and σ_β' form conjugate stresses. Derivation and proof of the conjugate stress principle can be found in Wood (1876).

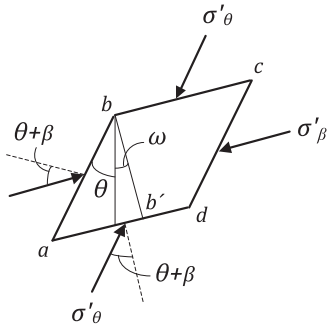

Fig. 2. Conjugate element and conjugate stress in soil element in backfill.

The stress state on the soil element consists of σ_θ' on planes bc and ad, and σ_β' on planes ab and cd. σ_θ' is obtained through

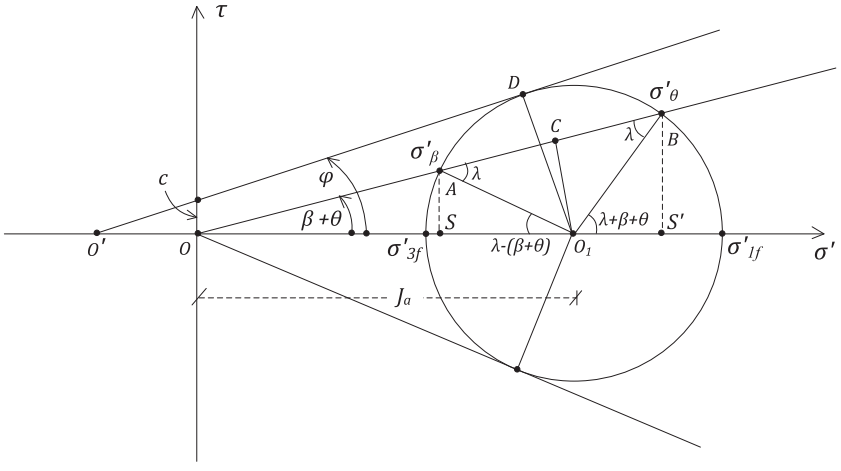

Fig. 3. The Mohr circle corresponding to conjugate stress state.

Eq. (4), and σ_β' may be determined through the Mohr circle representation of the stress state (Fig. 3). The circle corresponds to a state of failure determined by the Mohr–Coulomb failure criterion, where the major and minor principle stresses at failure are σ_{1f}' and σ_{3f}', respectively. The conjugate stress state in Fig. 3 can be determined on the Mohr circle by projecting a line through the origin, O, at an angle $(\beta+\theta)$ to the horizontal plane (Murthy, 2003; Lancellotta, 2009). σ_θ' and σ_β' are then determined by the two intersections of the projected line with the Mohr circle. There are a number of ways to determine σ_β' using the Mohr circle in Fig. 3; one approach is as follows:

$$\frac{\sigma_\beta'}{\sigma_\theta'}=\frac{OA}{OB}=\frac{AS}{BS'}=\frac{\sin(\lambda-(\beta+\theta))}{\sin(\lambda+(\beta+\theta))}=\frac{\cos(\beta+\theta)-\sin(\beta+\theta)\cot(\lambda)}{\cos(\beta+\theta)+\sin(\beta+\theta)\cot(\lambda)} \tag{5}$$

$$BS'=\sigma_\theta'\sin(\beta+\theta)=\gamma z(1\pm k_v)\frac{\cos\beta}{\cos\theta}\sin(\beta+\theta) \tag{6}$$

Letting $OO_1=J$, it follows that

$$O_1S'=OS'-OO_1=\gamma z(1\pm k_v)\frac{\cos\beta}{\cos\theta}\cos(\beta+\theta)-J \tag{7}$$

$$\tan(\lambda+(\beta+\theta))=\frac{\tan(\lambda)+\tan(\beta+\theta)}{1-\tan(\lambda)\tan(\beta+\theta)}=\frac{BS'}{O_1S'}=\frac{\gamma z(1\pm k_v)\cos\beta\sin(\beta+\theta)}{\gamma z(1\pm k_v)\cos\beta\cos(\beta+\theta)-J\cos\theta} \tag{8}$$

multiplying and rearranging, we get

$$\cot\lambda=\left(\frac{\gamma z\cos(\beta)(1\pm k_v)(\cos(\beta+\theta)+\sin(\beta+\theta)\tan(\beta+\theta))}{J\cos(\theta)}-1\right)\cot(\beta+\theta) \tag{9}$$

Substituting Eq. (9) into Eq. (5) and simplifying it, we obtain

$$\frac{\sigma_\beta'}{\sigma_\theta'}=\frac{2\cos\theta\cos(\theta+\beta)}{\gamma z(1\pm k_v)\cos\beta}J-1 \tag{10}$$

To get J, we have $BO_1=DO_1$ and $BO_1^2=O_1S'^2+BS'^2$, where

$$DO_1=(c\cot\varphi+J)\sin\varphi \tag{11}$$

Hence,

$$(c\cos\varphi+J\sin\varphi)^2=\left(\gamma z(1\pm k_v)\frac{\cos\beta}{\cos\theta}\cos(\beta+\theta)-J\right)^2+\left(\gamma z(1\pm k_v)\frac{\cos\beta}{\cos\theta}\sin(\beta+\theta)\right)^2 \tag{12}$$

Solving Eq. (12) for J, and noting that active condition J_a is equal to the smaller of the two roots,

$$J_a=\frac{1}{\cos^2\phi}\left(\left(\frac{\gamma z\cos\beta\cos(\beta+\theta)(1\pm k_v)}{\cos\theta}+c\cos\phi\sin\phi\right)-\sqrt{\gamma^2z^2\cos^2\beta(1\pm k_v)^2\left(\frac{\cos^2(\beta+\theta)-\cos^2\phi}{\cos^2\theta}\right)+c^2\cos^2\phi+\frac{2c\gamma z\cos\phi\sin\phi\cos\beta\cos(\beta+\theta)(1\pm k_v)}{\cos\theta}}\right) \tag{13}$$

Once the stresses on the conjugate planes have been determined, one can obtain the stress states on any other plane using the Mohr circle of stresses or the ellipse of stresses (Cain, 1916). The solution obtained in Eq. (10) is identical to the Rankine type of static solutions, including Rankine (1857), Chu (1991) and Mazindrani and Ganjali (1997) for both cohesionless ($c=0$, $\theta=0^\circ$) and cohesive soils ($\theta=0^\circ$), which further supports the generalized nature of the derived solution.

Consider the soil element depicted in Fig. 4, which is a prism formed by slicing the conjugate soil element in Fig. 2 along line bb' parallel to the wall. The stress state on the prism is comprised of σ_θ' and σ_β', which are the conjugate stresses already determined by Eqs. (4) and (10). The obliquity of conjugate stresses σ_θ' and σ_β' is $(\beta+\theta)$ as shown in Fig. 4. σ_a' is the stress acting on the wall and α is its orientation with respect to the normal of the wall. The prism under consideration is in a pseudo-static equilibrium under the applied stresses. σ_a' can be obtained by considering the force equilibrium of the prism along the direction normal to the wall (normal to bb') and taking the length of ab equal to the unit length in Fig. 4, as follows:

$$\sigma_a'\cos\alpha\frac{\cos(\beta+\theta)}{\cos(\beta-\omega)}=\sigma_\theta'\frac{\sin^2(\theta+\omega)}{\cos(\beta-\omega)}+\sigma_\beta'\cos(\beta-\omega) \tag{14}$$

Combining Eq. (14) with Eqs. (4) and (10), and manipulating the resulting expression, yields

$$\sigma_a'=\gamma zK_a=\gamma z\left(\frac{\cos\beta(1\pm k_v)(\sin^2(\theta+\omega)-\cos^2(\beta-\omega))}{\cos\alpha\cos(\beta+\theta)\cos(\theta)}+\frac{2(J_a/\gamma z)\cos^2(\beta-\omega)}{\cos\alpha}\right) \tag{15}$$

$$K_a=\frac{\cos\beta(1\pm k_v)(\sin^2(\theta+\omega)-\cos^2(\beta-\omega))}{\cos\alpha\cos(\beta+\theta)\cos(\theta)}+\frac{2(J_a/\gamma z)\cos^2(\beta-\omega)}{\cos\alpha} \tag{16}$$

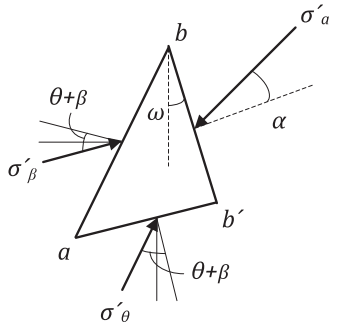

Fig. 4. Prism used to derive lateral earth pressure from conjugate stress planes.

The obliquity of the earth thrust, α_a, can be obtained by considering the equilibrium of the prism in the vertical direction, as follows:

$$\sigma_a' \sin\alpha \frac{\cos(\beta+\theta)}{\cos(\beta-\omega)} = \sigma_\theta' \frac{\cos(\theta+\omega)\sin(\theta+\omega)}{\cos(\beta-\omega)} + \sigma_\beta' \sin(\beta-\omega) \quad (17)$$

α_a is assumed to be constant in most earth pressure solutions (e.g., Coulomb assumes $\alpha=\delta=2/3\varphi$). The obliquity can be calculated in the proposed formulation by dividing Eq. (17) by Eq. (14) yielding α_a for the active condition as

$$\alpha_a = \tan^{-1}\left(\frac{\left(\frac{2\cos\theta\cos(\beta+\theta)}{\cos\beta(1\pm k_v)}\frac{J_a}{\gamma z}-1\right)\sin 2(\beta-\omega)+\sin 2(\theta+\omega)}{2\left(\left(\frac{2\cos\theta\cos(\beta+\theta)}{\cos\beta(1\pm k_v)}\frac{J_a}{\gamma z}-1\right)\cos^2(\beta-\omega)+\sin^2(\theta+\omega)\right)}\right) \quad (18)$$

$$\sigma_{AEH}' = \sigma_a' \cos(\alpha_a+\omega) \quad (19)$$

Contrary to the conventional assumption of a constant obliquity, α_a from the proposed solution is a function of problem geometry, pseudo-static accelerations and soil properties; it varies with depth. The proposed formulation is illustrated in Fig. 5, where a practical example incorporating seismic loading, wall inclination and backfill slope is presented for c–φ backfill. The resulting stress distribution is nonlinear due to the quadratic form of the formulation. Additionally, the computed values for the friction angle of the active soil wall in Fig. 5 decrease with depth, due to the contribution of cohesion. In particular, the cohesion term in Eq. (13) results in an increase in J_a with depth, leading to a decrease in the soil–wall friction angle, as predicted by Eq. (18).

3. Horizontal thrust

The depth of a tension crack can be determined by setting Eq. (19) to zero and solving the quadratic function in terms of z. The exact solution is extremely long and impossible to implement by hand. However, a linear regression analysis of the repeated representative trials revealed that the σ'_{AEH} can be closely approximated using a linear distribution, with an R^2 in the range of 0.95–0.99. Hence, a good approximation of z_c can be determined as follows:

$$z_c = H'\left(1-\frac{0.9\sigma_{AEH(z=H')}'}{\sigma_{AEH(z=H')}'-\sigma_{AEH(z=0.1H')}'}\right) \quad (20)$$

$$H' = H\frac{\cos(\beta-\omega)}{\cos\beta\cos\omega} \quad (21)$$

where H' is the vertical distance between the heel of the retaining wall and its backfill slope surface (Fig. 1).

The net value of the horizontal seismic earth thrust, P_{AEH}, as well as the point of its application can be obtained through the numerical integration of the lateral thrust (Eq. 19) along the length of the wall minus the length of the tension crack. To simplify the problem, an acceptable approximation of the horizontal lateral earth thrust can be computed by considering the triangular stress distribution below the depth of the tension

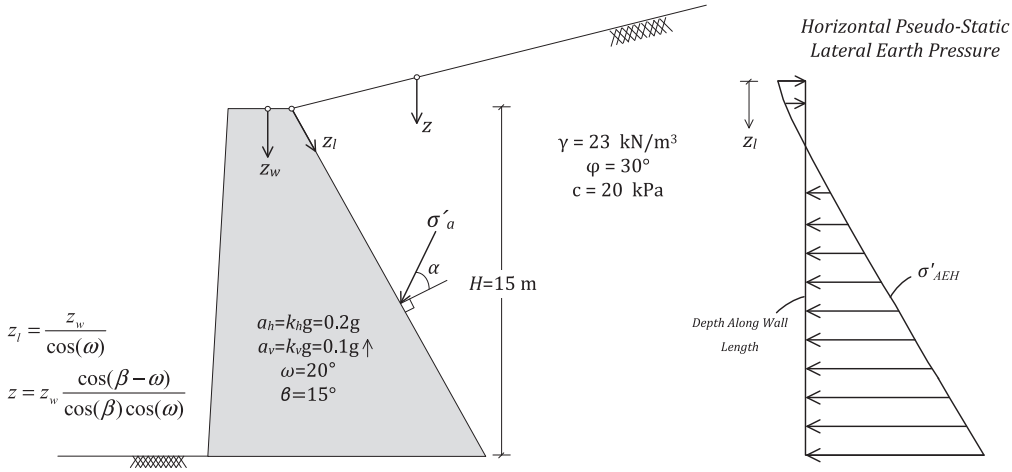

Z_w (m)	Depth Along Length of Wall, Z_l (m)	Z (m)	J_a (Eq. 13)	α_a (°) (Eq. 18)	K_a (Eq. 16)	σ'_a (kPa) (Eq. 15)	σ'_{AEH} (kPa) (Eq. 19)
0.0001	0.0001	0.0001	-11.55	-5.00	-9113	-23.01	-22.22
3.00	3.19	3.29	39.62	53.66	0.561	42.46	11.95
6.00	6.39	6.59	97.59	36.94	0.716	108.51	59.19
9.00	9.58	9.88	157.46	32.23	0.791	179.80	110.11
12.00	12.77	13.17	218.23	29.97	0.835	253.06	162.75
15.00	15.96	16.46	279.5	28.63	0.865	327.37	216.35

Fig. 5. Illustrative example of inclined wall retaining sloped c–φ backfill.

crack only (Fig. 6(a)), since the distribution of σ'_{AEH} is found to be nearly linear along the wall.

$$P_{AEH} = \frac{1}{2}\sigma_{AEH(z=H')}{}'\left(H_l - z_c \frac{\cos\beta}{\cos(\beta-\omega)}\right) \quad (22)$$

$$H_l = \frac{H}{\cos(\omega)} \quad (23)$$

where H_l is the length of the wall and the point of application of the horizontal active earth thrust P_{AEH} is at $1/3(H_l - z_c \cos(\beta)/\cos(\beta-\omega))$ along the length of the wall.

Richards and Shi (1994) pointed out that when a tension crack occurs, the weight and the inertial force above the cracked depth should be considered as applied tractions; it is unconservative to ignore the weight of the soil above the cracked depth in the analysis. They found that the resulting horizontal earth thrust, including the effect of the weight of the soil above the cracked depth, is nearly the same as the resulting horizontal earth thrust assuming that $\sigma_{AEH}{}'$ follows a linear trend from the heel to the top of the wall. Hence, a more conservative approximation of the horizontal component of the lateral earth thrust is shown in Fig. 6(b).

$$P_{AEH} = \frac{1}{2}\sigma_{AEH(z=H')}{}' H_l \quad (24)$$

The point of application of horizontal active earth thrust P_{AEH} is at $1/3H_l$ along the length of the wall. The horizontal earth thrust for the example depicted in Fig. 5 is shown for both assumptions in Fig. 6(a) and (b).

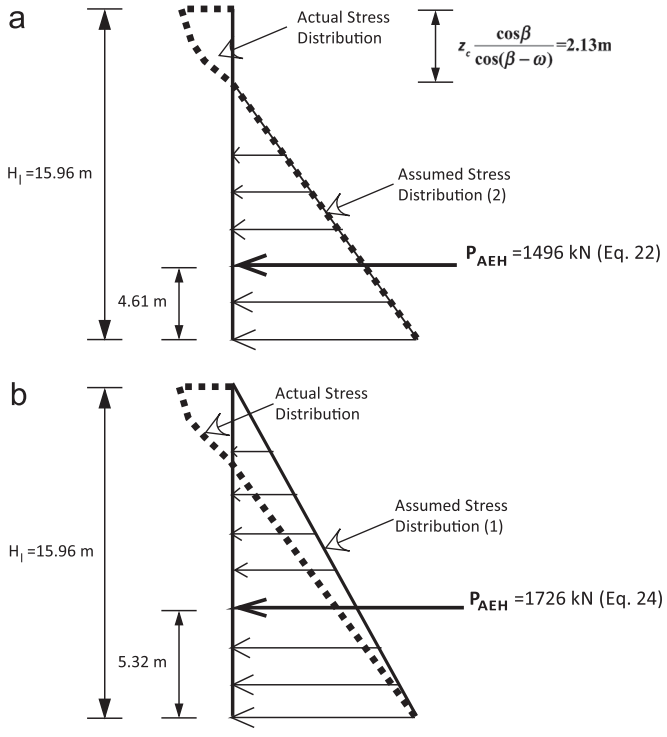

Fig. 6. Actual and assumed stress distributions in illustrative example, along with values for calculated parameters.

4. Comparison with available solutions

Case 1. static analysis

The proposed formulation was validated through a comparison with other available solutions. For the static case ($\theta=0^\circ$), Tables 1 and 2 show comparisons of the active lateral earth pressure coefficient K_a obtained from the proposed formulations with several published methods. Inherent to the proposed solution, the soil–wall friction angle is directly calculated as a function of the problem geometry and inertia, as opposed to being assumed as an independent constant in the Coulomb-type solutions. It can be seen from Table 1 for vertical walls with cohesionless backfill that the computed soil–wall friction angle is independent of the soil friction angle, but equal to the backfill slope, as expected for Rankine-type solutions. Since soil wall friction angle δ in the Coulomb-type solutions is not directly calculated, but assumed as a fraction of soil friction angle φ, to facilitate the comparison, δ is chosen to be equal to (i) α_a obtained from the proposed solution and (ii) $2/3\varphi$ commonly assumed in practice. The proposed solution yielded identical results to other solutions for cohesionless soil with $\delta=\alpha_a$, and the minor difference between the proposed solution and Mazindrani and Ganjali's solution for c–φ soils when the backfill is sloped is due to the different ways that K_a is defined. Assuming $\delta=2/3\varphi$, the values for K_a, obtained from Coulomb, are lower than those obtained from the proposed method, since the soil–wall friction angle assumed in the Coulomb method, is higher than the α_a computed in the proposed method.

Although recent numerical analyses (Evangelista et al., 2010) support adopting a soil–wall friction angle dependent on inertial forces, experimental measurements to justify the adoption of an inertia-dependent or constant soil–wall friction angle are lacking. If the mobilized soil–wall interface friction angle under seismic loading is indeed to be a function of the problem geometry and inertia, the proposed solution may serve as a benchmark for developing realistic values for mobilized interface friction.

Case 2. seismic analysis of cohesionless soil ($c=0$)

For cohesionless soil, $c=0$ can be substituted into Eq. (13) and J_a can be simplified as follows:

$$J_{a(c=0)} = \frac{\gamma z \cos\beta(1\pm k_v)(\cos(\beta+\theta) - \sqrt{\cos^2(\theta+\beta) - \cos^2\phi})}{\cos^2\phi \cos\theta} \quad (25)$$

The simplified $J_{a(c=0)}$ is linearly proportional to z, which means $J_{a(c=0)}/\gamma z$ is a constant. As a result, both α_a and K_a become constants and σ'_{AEH} is linearly proportional to z, as expected for cohesionless soil. This is attractive since, for cohesionless soil, the proposed solution can thus accommodate layered soil profiles and the presence of groundwater, which require a tedious analysis in the Coulomb-type solutions. An example is shown in Fig. 7 to illustrate the application.

The horizontal component of the seismic lateral earth thrust, computed using the proposed formulation, has been compared with that computed using the M–O method and the stress-based solution derived by Mylonakis et al. (2007) for the case of $c=0$. The soil wall friction angle has to be assumed in both

Table 1
Comparison of static active lateral earth pressure coefficient for cohesionless soil with vertical walls.

Backfill slope β (deg)		0			15
Soil-wall friction angle α_a (deg)		0			15
Soil friction angle φ (deg)		20	30	40	30
The proposed method	K_a	0.490	0.333	0.217	0.373
Rankine (1857)		0.490	0.333	0.217	0.373
Coulomb (1776) ($\delta=\alpha_a$)		0.490	0.333	0.217	0.373
Coulomb (1776) ($\delta=2/3\varphi$)		0.438	0.297	0.200	0.371

Table 2
Comparison of static active lateral earth pressure coefficient for c–φ soil.

$\theta=0^\circ$, $\omega=0^\circ$, $\varphi=30^\circ$	K_a			
Backfill slope β (deg)	0		15	
Cohesion $c/\gamma z$	0.05	0.5	0.05	0.5
The proposed method	0.276	−0.244	0.304	−0.254
Mazindrani and Ganjali (1997)	0.276	−0.244	0.315	−0.263

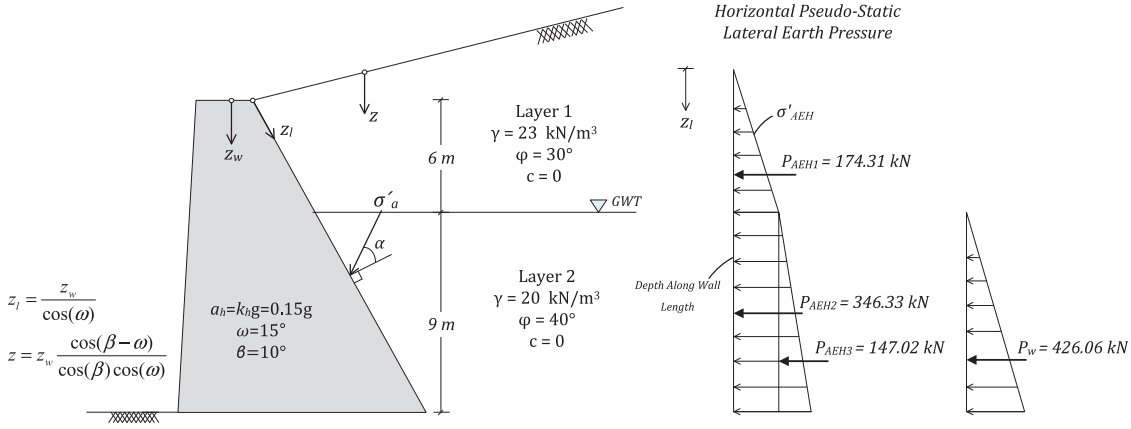

Z_w (m)	Depth Along Length of Wall, Z_l (m)	Z (m)	J_a (Eq. 13)	α_a (°) (Eq. 18)	K_a (Eq. 16)	σ'_a (kPa) (Eq. 15)	σ'_{AEH} (kPa) (Eq. 19)
0.0001	0.0001	0.0001	0.75	29.7	0.698	0	0
6.00 (Layer 1)	6.21	6.28	0.75	29.7	0.698	78.98	56.14
6.00 (Layer 2)	6.21	6.28	0.69	39.56	0.567	64.09	37.16
15.00	15.53	15.71	0.69	39.56	0.567	118.51	68.71

Fig. 7. Illustrative example of inclined wall retaining sloped and layered cohesionless backfill with ground water.

Table 3
Comparison of seismic lateral earth pressure between proposed method and other solutions ($\delta=\alpha_a$ and $\delta=2/3\varphi$).

$c=0$, $\omega=20^\circ$, $\beta=15^\circ$, $K_v=0$		$P^*_{AE}=P_{AEH}/\gamma H^2$					
Soil friction angle φ (deg)		35			40		
Horizontal seismic coefficient K_h		0.1	0.2	0.3	0.1	0.2	0.3
The proposed method		0.230	0.326	0.501	0.184	0.261	0.381
M–O method	$\delta=\alpha_a$	0.230	0.326	0.501	0.184	0.261	0.381
	$\delta=2/3\varphi$	0.250	0.333	0.498	0.206	0.271	0.378
Mylonakis et al. (2007)	$\delta=\alpha_a$	0.230	0.338	0.570	0.185	0.271	0.427
	$\delta=2/3\varphi$	0.270	0.377	0.583	0.226	0.313	0.456

the M–O method and Mylonakis et al.'s (2007) solution, whereas it is determined analytically using Eq. (18) in the proposed method. To facilitate the comparison, the soil–wall friction angle in the M–O method and Mylonakis solution have been assumed equal to (1) $\delta=2/3\varphi$ in Tables 3 and (2) $\delta=\alpha_a$ in Fig. 8. It can be seen that the values for P^*_{AE}, obtained from the M–O method and Mylonakis's solution assuming $\delta=2/3\varphi$, are generally higher than those obtained from the proposed method (Table 3). In addition, under the assumption of $\delta=\alpha_a$, the proposed solution and the M–O solution converge to identical results in all situations (Fig. 8), whereas the solution by Mylonakis predicts higher earth pressure for non-vertical walls with sloped backfill. Iskander et al. (2012) reported similar findings.

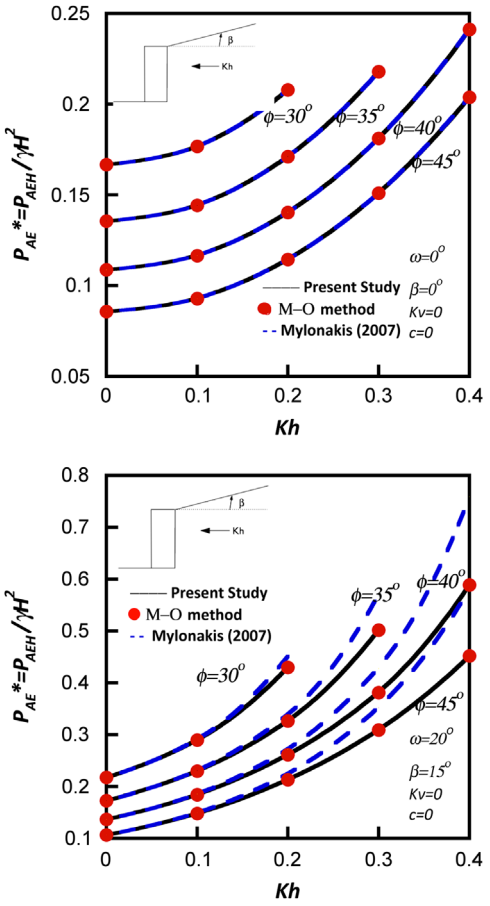

Fig. 8. Comparison between the proposed method and other solutions for cohesionless backfill ($\delta=\alpha_a$).

A further comparison of the proposed solution was made (Table 4) with the elasto-dynamic method proposed by Psarropoulos et al. (2005), as well as with the widely used method suggested by Seed and Whitman (1970), for a representative case of $c=0$, $\beta=0^\circ$, $\omega=0^\circ$, $\phi=30^\circ$, $K_h=0.15$ and $K_v=0$. The elasto-dynamic solution can be applied to both rigid and flexible walls, by specifying wall flexibility (d_w) and base flexibility (d_θ) terms. The proposed solution is in good agreement with the method proposed by Seed and Whitman (1970), as well as with the elasto-dynamic method in the case of high base flexibility ($d_\theta=5$). In the case of the rigid base ($d_\theta=0$), the proposed solution as well as that of Seed and Whitman (1970) deviate from the elasto-dynamic solution due to the difference in inherent assumptions in the various methods. In particular, the proposed solution is applicable to walls with sufficient base flexibility which allow active conditions to be achieved in the backfill.

Case 3. seismic analysis of c–φ soils

A comparison between the proposed method and the previously published work for c–φ soils is difficult. None of the existing solutions considers all the factors included in the proposed method; therefore, a comparison is made for conditions where solutions are available ($\beta=0^\circ$ and $\omega=0^\circ$). The two dimensionless parameters, c^* and P^*_{AE}, are employed to

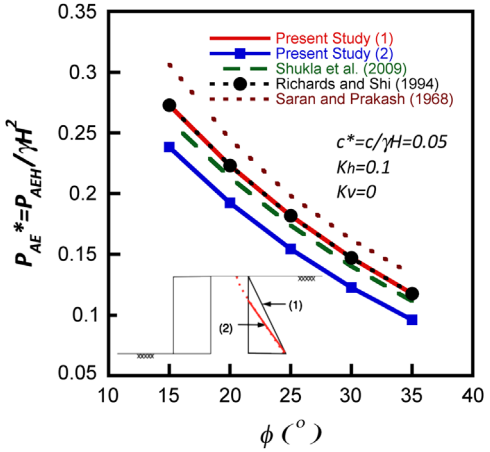

Fig. 9. Comparison of the proposed method with other methods from literature for P^*_{AE} against φ.

Table 4
Comparison of normalized lateral earth pressure from various methods.

$c=0$, $\omega=0^\circ$, $\beta=0^\circ$, $\varphi=30^\circ$, $K_v=0$, $K_h=0.15$	$P^*_{AE}=P_{AEH}/\gamma H^2$					
The proposed method	0.190			0.190		
Seed and Whitman (1970)	0.223			0.223		
Psarropoulos et al. (2005)	$d_\theta=0$			$d_\theta=5$		
	$d_w=0$	$d_w=5$	$d_w=40$	$d_w=0$	$d_w=5$	$d_w=40$
	0.321	0.268	0.233	0.221	0.220	0.213

d_θ: flexibility of the rotational base.
d_w: flexibility of the wall.

facilitate comparisons as follows:

$$c^* = \frac{c}{\gamma H} \tag{26}$$

$$P^*_{AE} = \frac{P_{AEH}}{\gamma H^2} \tag{27}$$

A comparison of the proposed method has been made with other published methods for $c^*=0.05$, $K_h=0.1$ and $K_v=0$ in Fig. 9. The value for P^*_{AE}, obtained from the proposed method, is consistent with the previously published methods. P^*_{AE} is obtained, based on the conservative stress distribution (assumption 1), and it is identical to that obtained from Richards and Shi (1994), but lower than that obtained from Saran and Prakash (1968) and slightly higher than that obtained from Shukla et al. (2009) for the range in friction angles (15–35°) and cohesion considered. When employing the triangular stress distribution below the tension crack (assumption 2), P^*_{AE} is obtained based on the proposed method and is lower than all other methods for the same set of parameters. The variation in total horizontal active thrust P^*_{AE} is plotted against K_h for $c^*=0.05$, $\varphi=30^\circ$ and $K_v=0$ and ± 0.1 in Fig. 10. Again, the results of the proposed method are consistent with the available ones. The difference between the proposed results and those obtained from Richards and Shi, when $K_v=\pm 0.1$, is due to a missing term for $(1\pm K_v)$ in Richards and Shi's derivation. The effect of cohesion on the computed lateral thrust is illustrated in Fig. 11 for $\varphi=30^\circ$, $K_h=0.2$ and $K_v=0$. Based on the more conservative stress distribution (assumption 1), the P^*_{AE} computed using the proposed method is identical to Richards and Shi (1994) and somewhat different from Shukla et al. (2009) and Saran and Prakash (1968) due to the difference in the assumptions involved. Based on the stress distribution (2), the P^*_{AE} obtained

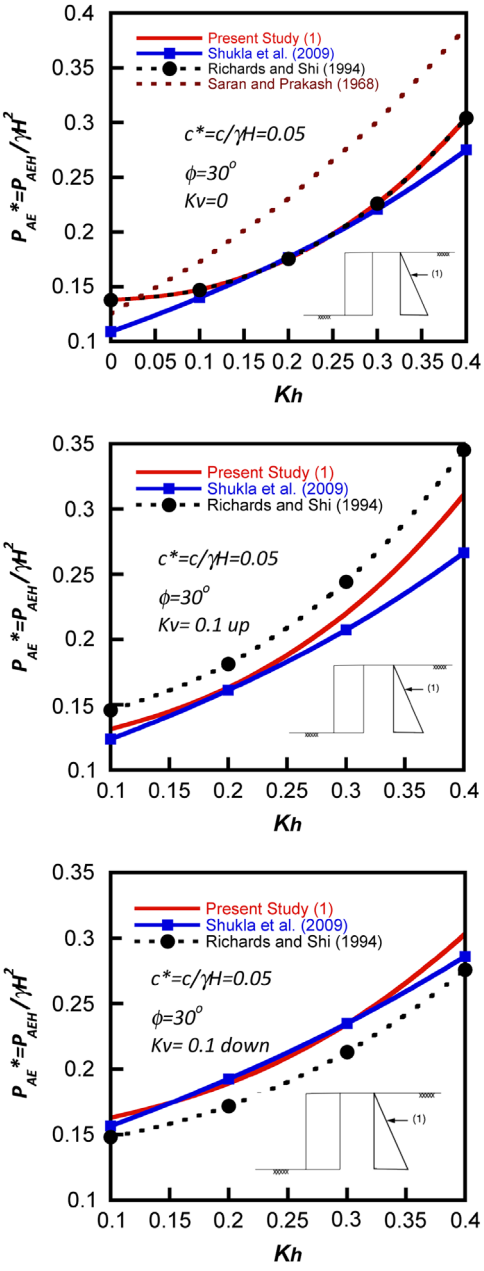

Fig. 10. Comparison of the proposed method with other methods from literature for P^*_{AE} against K_h for $K_v=0$ and $K_v=\pm 0.1$.

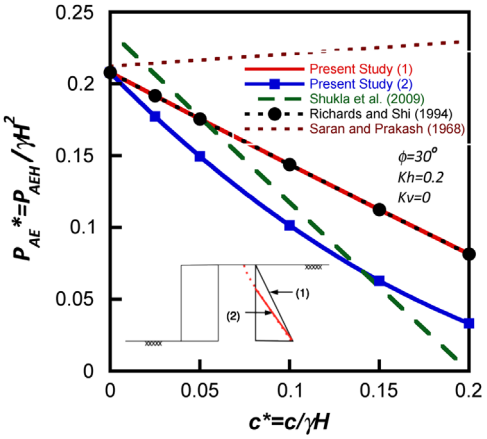

Fig. 11. Comparison of the proposed method with other methods from literature for P^*_{AE} against c^*.

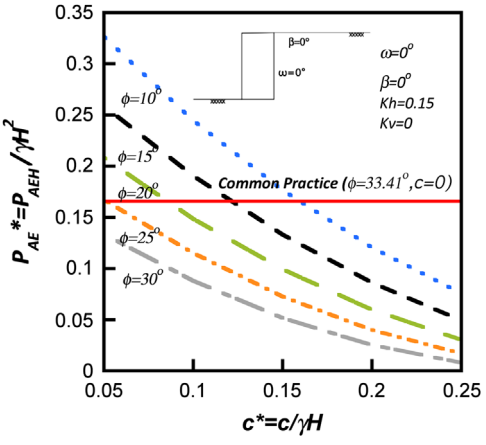

Fig. 12. Comparison of the proposed method with common practice* (substitute c–φ soil with cohesionless soil with $\varphi=33.41^\circ$).

from the present study is lower than all other methods, except when c^* is greater than 0.15 where it is higher than that of Shukla et al. (2009). Huntington (1957) noted: "*For many years it was almost universal practice to compute the earth pressure against a retaining wall on the assumption that the soil was cohesionless and that the value of φ could be considered equivalent to the angle of repose…. The most common assumption according to this practice was that the slope of the angle of repose was 1.5 horizontal: 1 Vertical*" (i.e., 33.4°). Fig. 12 shows that the aforementioned practice leads to the significant overdesign for low walls and under-design for high walls.

Case 4. seismic analysis of undrained cohesive soil ($\varphi=0$)

Anderson et al. (2008) suggested that total stress strength parameters for c–φ soils, based on undrained triaxial tests, should be used to compute the seismic lateral earth pressure. For the total stress analysis, $\varphi=0$ is substituted into Eq. (13) and J_a is simplified as follows:

$$J_{a(\varphi=0)} = \frac{\gamma z \cos\beta \cos(\beta+\theta)(1\pm k_v)}{\cos\theta} - \sqrt{\gamma^2 z^2 \cos^2\beta(1\pm k_v)^2\left(\frac{\cos^2(\beta+\theta)-1}{\cos^2\theta}\right)+c^2} \quad (28)$$

Unlike cohesionless soils, $J_{a(\varphi=0)}$ is nonlinear against z. As a result, the horizontal stress distribution is nonlinear against z. It should be noted that the approximated linear distribution of σ_{AEH}' does not hold for the total stress analysis. On the contrary, σ_{AEH}' was found to closely follow a second order polynomial. Therefore, the horizontal stress distribution against the length of the wall can be plotted with depth using Eq. (19) and the equation of the second order polynomial fit can be employed to obtain the exact depth of the tension crack, as depicted in the example shown in Fig. 13. The net value of the horizontal seismic earth thrust, P_{AEH}, and the point of its application for the aforementioned example are obtained by integrating the resulting polynomial equation (below the tension crack), as follows:

$$P_{AEH} = \int_{7.59}^{10.15} \sigma_{AEH}'(z_l)dz_l = 139.64 \text{ kN} \quad (29)$$

$$\text{Point of application} = \frac{\int_{7.59}^{10.15} z_l\sigma_{AEH}'(z_l)dz_l}{P_{AEH}} = 9.31 \text{ m} \quad (30)$$

There are no suitable closed-form solutions for comparison; thus, the solution is validated by examining the static cases and the case of the c–φ soil. Alternatively, conventional limit-equilibrium slope stability computer programs, such as SLIDE (RocScience, 2005), may be employed to perform a total stress analysis under seismic conditions.

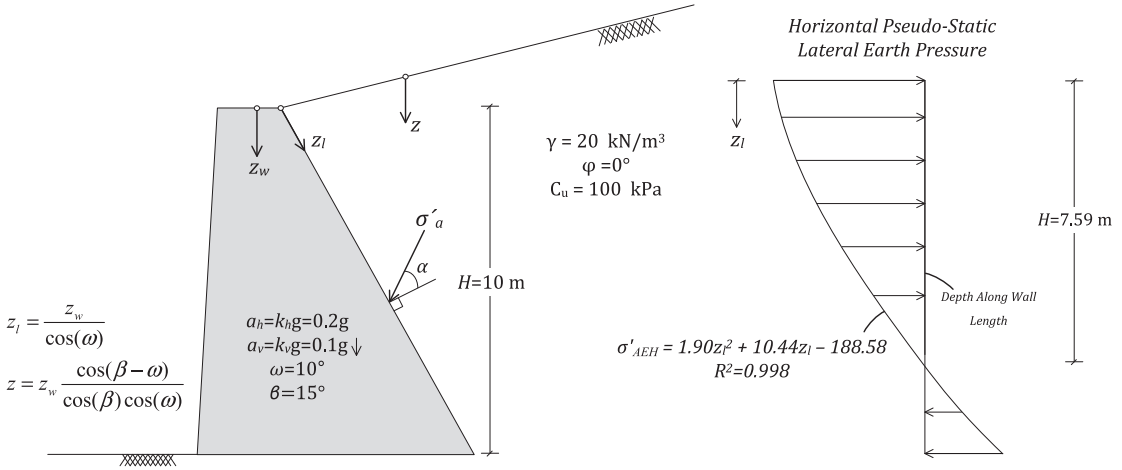

Z_w (m)	Depth Along Length of Wall, Z_l (m)	Z (m)	J_a (Eq. 13)	α_a (°) (Eq. 18)	K_a (Eq. 16)	σ'_a (kPa) (Eq. 15)	σ'_{AEH} (kPa) (Eq. 19)
0.0001	0.0001	0.0001	-99.99	5.00	-95100	-199.24	-192.45
2.00	2.03	2.09	-57.22	-0.73	-3.753	-157.21	-155.16
4.00	4.06	4.19	-10.42	-11.55	-1.315	-110.09	-110.15
6.00	6.09	6.28	41.24	-41.23	-0.519	-65.22	-55.77
8.00	8.12	**8.38**	100.21	69.51	0.415	69.57	12.67
10.00	10.15	10.47	178.94	33.53	0.785	164.34	119.15

Fig. 13. Illustrative example for total stress analysis.

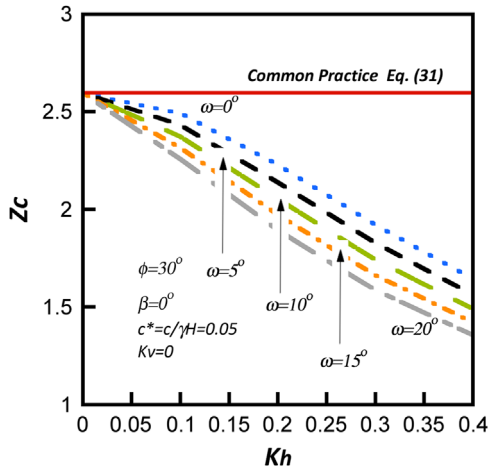

Fig. 14. Effect of K_h and ω on depth of tension crack (Z_c).

5. Design considerations

5.1. Tension crack

The effect of tension cracks is quite important in active earth pressure problems. The depth of tension crack Z_c, behind vertical wall retaining c–φ soils, is generally given for static loading by the following formula:

$$z_c = \frac{2c}{\gamma} \tan\left(45^\circ + \frac{\varphi}{2}\right) \tag{31}$$

Eq. (31) is sometimes employed in seismic analysis as a rough approximation of the tension crack under seismic conditions (Huntington, 1957). Fig. 14 shows the combined effect of horizontal seismic acceleration K_h and wall inclination ω on the depth of tension crack Z_c using the proposed formulation. Z_c decreases with both K_h and ω, which also indicates that Eq. (31) will significantly overestimate the depth of the tension crack for c–φ backfill under seismic conditions.

6. Vertical seismic acceleration

The effect of vertical seismic coefficient K_v is generally ignored in seismic earth pressure problems. For situations where K_v is considered, it is almost a universal rule to consider K_v in the upward direction (Das and Ramana 2011; Kramer, 1996). The effect of the vertical acceleration is explored in Fig. 15, where P^*_{AE} is plotted for both upward and downward accelerations. P^*_{AE}, obtained using the proposed method, is higher when K_v is in the downward direction in most cases, except when K_h is extremely large ($K_h \approx 0.4$). This is observed when $K_h \leq 0.3$, because the increase in the seismic force due to the term $(1+K_v)$ in Eq. (15) with downward acceleration overcomes the decrease in force due to the reduction in angle θ of the pseudo-static acceleration field. Hence, an upward vertical acceleration would actually result in a lower active lateral earth pressure against a rigid retaining wall. Nevertheless, an upward acceleration may effectively reduce the weight of the retaining wall, which may result in reduced stability. Thus, both cases should be analyzed, particularly for

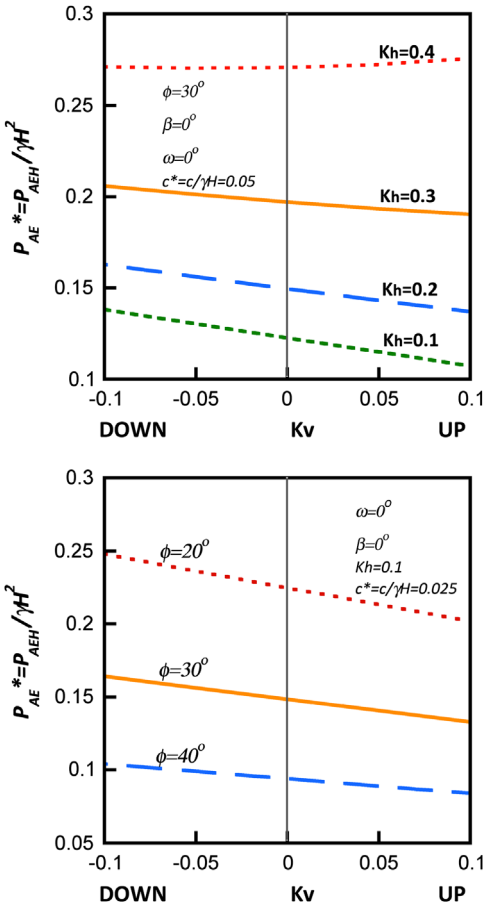

Fig. 15. Variation in P^*_{AE} as a function of K_v for wide range of K_h and φ from the proposed method.

walls having uncommon geometries. In any case, the stresses adjacent to the wall are expected to be different from those of the free field (Richards et al., 1999; Paik and Salgado, 2003), which is disregarded in this study, following Rankine's original assumptions that the stress field adjacent to the wall is the same as that in the free field.

6.1. Design charts

Design charts are presented in Figs. 16 and 17 to compute P^*_{AE} for a range in scenarios involving different combinations of K_h, c^*, φ, β and ω. These design charts can be useful tools for practicing engineers to design many retaining wall problems.

7. Conclusions

The present study has presented a generalized analytical expression to compute the static and pseudo-static seismic active lateral earth pressure on retaining walls supporting c–φ soils, based on an extension of Rankine's conjugate stress principle. The proposed method is the only available solution, which accounts for the soil–wall friction angle, the depth of the tension crack, the wall inclination and the sloped backfill for the pseudo-static analysis of c–φ backfill. Unlike force-based

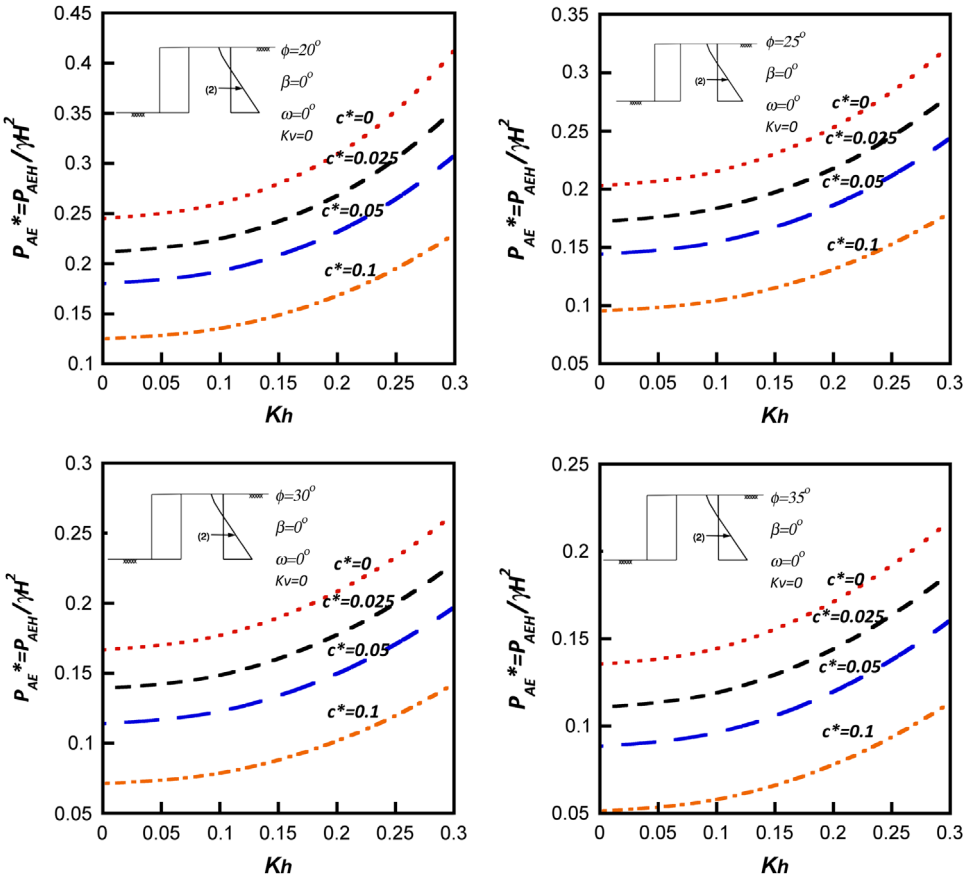

Fig. 16. Design charts to compute P_{AE}^* for wide range of K_h, φ and c^*.

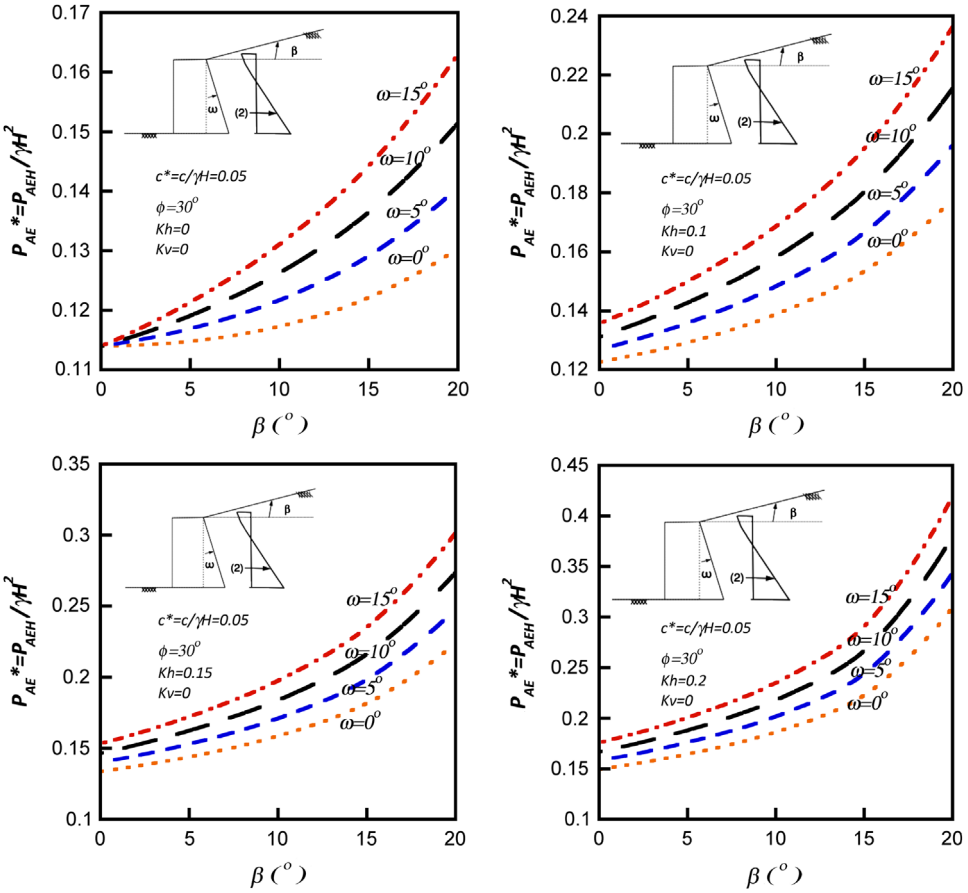

Fig. 17. Design charts to compute P_{AE}^* for wide range of β, ω and K_h.

methods, the proposed method provides a stress-based solution where the distribution of the net active thrust is easily obtained. The results from the proposed formulation compare favorably with existing methods for situations where a comparison is feasible. In addition, both depth of the tension crack and the soil–wall friction angle are calculated directly within the proposed expressions, whereas they must be approximated or assumed in most formulations. Design charts have been presented to calculate the net active horizontal thrust from c–φ backfill on retaining walls for different scenarios.

Acknowledgments

The authors gratefully acknowledge the support of the Defense Threat Reduction Agency (DTRA) Grant no. HDTRA1-10-1-0049 and the National Science Foundation (NSF) grant DGE 0741714.

Appendix

Nomenclature

a_h horizontal acceleration
a_v vertical acceleration
k_h horizontal seismic coefficient
k_v vertical seismic coefficient
α_a active soil–wall friction angle in the proposed method
β backfill surface slope
δ soil wall friction angle in Mononobe–Okabe method
γ soil unit weight
γ_θ soil unit weight in the direction of z_θ (see Fig. 1)
θ orientation of the pseudo-static acceleration field (see Fig. 1)
φ soil internal friction angle
c soil cohesion
ω wall inclination with respect to the vertical
g gravitational acceleration
g_θ resultant of the gravitational acceleration and pseudo-static vertical and horizontal acceleration (see Fig. 1)
H wall height
H_l wall length
H' distance between heel of retaining wall and its backfill slope (see Fig. 1)
J_a simplifying term for active lateral earth pressure
K_a active seismic lateral earth pressure coefficient
$\sigma_a{}'$ resultant stress acting on soil prism adjacent to wall (see Fig. 4)
W weight of soil over conjugate stress element
$\sigma_\beta{}'$ lateral component of effective stress on conjugate stress element parallel to backfill slope surface (see Fig. 2)
$\sigma_\theta{}'$ conjugate component of effective stress on conjugate stress element along θ axis (see Fig. 2)
$\sigma_{1f}{}'$ major principle stress at failure under active conditions (see Fig. 3)
$\sigma_{3f}{}'$ minor principle stress at failure under active conditions (see Fig. 3)
z vertical depth of soil element from backfill surface
z_l vertical depth along wall length
z_w vertical depth from top of wall surface
z_θ Z axis direction rotated clockwise to angle of θ

References

Al-Homoud, A.S., Whitman, R.V., 1994. Comparison between FE prediction and results from dynamic centrifuge tests on tilting gravity walls. Soil Dynamics and Earthquake Engineering 14 (323), 259–268.

Anderson, D.G., Martin, G.R., Lam, I.P., Wang, J.N., 2008. Seismic Design and Analysis of Retaining Walls, Buried Structures, Slopes and Embankments, NCHRP Report 611. Transportation Research Board, National Cooperative Highway Research Program, Washington DC.

Cain, W., 1916. Earth Pressure, Retaining Walls and Bins, John Wiley and Sons, New York. Available from: ⟨books.google.com⟩ (accessed 03.07.11.).

Caquot, A., Kerisel, J., 1948. Tables for the Calculation of the Passive Pressure, Active Pressure and Bearing Capacity of Foundations. Gauthier-Villars, Paris.

Chu, S.C., 1991. Rankine's analysis of active and passive pressures in dry sands. Soils and Foundations 31 (4), 115–120.

Das, B.M., Ramana, G.V., 2011. Principles of Soil Dynamics. Sengage Learning, Stamford, CT.

Evangelista, A., Santolo, A.S., Simonelli, A.L., 2010. Evaluation of pseudo-static active earth pressure coefficient of cantilever retaining walls. Soil Dynamics and Earthquake Engineering 30, 1119–1128.

Gazetas, G., Psarropoulos, P.N., Anastasapoulos, I., Gerolymos, N., 2004. Soil behavior of flexible retaining systems subjected to short-duration moderately strong excitation. Soil Dynamics and Earthquake Engineering 24, 537–550.

Ghosh, S., Sharma, R.P., 2010. Pseudo-dynamic active response of non-vertical retaining wall supporting c–φ backfill. Geotechnical and Geological Engineering 28 (5), 633–641.

Habibagahi, K., Ghahramani, A., 1979. Zero extension line theory of earth pressure. Journal of the Geotechnical Engineering Division, ASCE 105 (GT7), 881–896.

Heyman, J., 1997. Coulomb's Memoir on Statics: An Essay in the History of Civil Engineering. Imperial College Press, London.

Huntington, W.C., 1957. Earth Pressures and Retaining Walls. John Wiley and Sons, New York.

Iskander, M., Omidvar, M., Elsherif, O., 2012. Conjugate stress approach for Rankine seismic active earth pressure in cohesionless soils. Journal of Geotechnical and Geoenvironmental Engineering 139 (7), 1205–1210.

Koseki, J., Hong, K., Nakajima, S., Mulmi, S., Watanabe, K., Tateyama, M., 2010. Negative pore air pressure generation in backfill of retaining walls during earthquakes and its effect on seismic earth pressure. Soils and Foundations 50 (5), 747–755.

Kramer, S.L., 1996. Geotechnical Earthquake Engineering. Prentice Hall, New Jersey.

Lancellotta, R., 2007. Lower-bound approach for seismic passive earth resistance. Geotechnique 57 (3), 319–321.

Lancellotta, R., 2009. Geotechnical Engineering, second ed. Taylor & Francis, New York.

Lew, M., Sitar, N., Al Atik, L., Pourzanjani, M., Hudson, M.B., 2010a. Seismic earth pressure on deep building basements. In: Proceedings of the Annual Convention 2010, Structural Engineers Association of California.

Lew, M., Sitar, N., Al Atik, L., 2010b. Seismic earth pressures: fact or fiction. Invited Keynote Paper. In: Proceedings of Earth Retention Conference, ER 2010, ASCE, Seattle.

Madabhushi, S.P.G., Zeng, X., 2007. Simulating seismic response of cantilever retaining walls. Journal of Geotechnical and Geoenvironmental Engineering 133 (5), 539–549.

Mazindrani, Z.H., Ganjali, M.H., 1997. Lateral earth pressure problem of cohesive backfill with inclined surface. Journal of Geotechnical and Geoenvironmental Engineering 123 (2), 110–112.

Mononobe, N., Matsuo, M., 1932. Experimental Investigation of Lateral Earth Pressure During Earthquakes. Earthquake Research Institute and Research Office of Public Works, pp. 884–902.

Mononobe, N., Matsuo, O., 1929. On the determination of earth pressure during earthquakes. In: Proceeding of the World Engineering Congress, vol. 9, Tokyo, Japan, pp. 179–187.

Mylonakis, G., Kloukinas, P., Papantonopoulos, C., 2007. An alternative to the Mononobe–Okabe equations for seismic earth pressures. Soil Dynamics and Earthquake Engineering 27, 957–969.

Murthy, V.N.S., 2003. Geotechnical Engineering: Principles and Practices of Soil Mechanics and Foundation Engineering. Marcel Dekker, New York.

Nakamura, S., 2006. Reexamination of Mononobe–Okabe theory of gravity retaining walls using centrifuge model tests. Soils and Foundations 46 (2), 135–146.

Okabe, S., 1924. General theory on earth pressure and seismic stability of retaining walls and dams. Journal of Japanese Society of Civil Engineers 10 (6), 1277–1323.

Paik, K.H., Salgado, R., 2003. Estimation of active earth pressure against rigid retaining walls considering arching effects. Geotechnique 53 (7), 643–653.

Psarropoulos, P.N., Klonaris, G., Gazetas, G., 2005. Seismic earth pressures on rigid and flexible earth retaining walls. Soil Dynamics and Earthquake Engineering 25, 795–809.

Rankine, W.J.M., 1857. On the stability of loose earth. Philosophical Transactions of the Royal Society of London 147, 9–27.

Rankine, W.J.M., 1858. A Manual of Applied Mechanics, Glasgow University Press. Available from: ⟨books.google.com⟩ (accessed 03.07.11.).

Richards, R., Shi, X., 1994. Seismic lateral pressures in soils with cohesion. Journal of Geotechnical Engineering 120 (7), 1230–1251.

Richards, R., Huang, C., Fishman, K.L., 1999. Seismic earth pressure on retaining structures. Journal of Geotechnical and Geoenvironmental Engineering 125 (9), 771–778.

RocScience, 2005. Slide: Stability Analysis for Soil and Rock Slopes. ⟨www.rocscience.com⟩.

Saran, S., Gupta, R.P., 2003. Seismic earth pressures behind retaining walls. Indian Geotechnical Journal 33 (3), 195–213.

Saran, S., Prakash, S., 1968. Dimensionless parameters for static and dynamic earth pressures behind retaining walls. Indian Geotechnical Journal 7 (3), 295–310.

Seed, H.B., Whitman, R.V., 1970. Design of earth retaining structures for dynamic loads. In: Proceedings of the Specialty Conference on Lateral Stresses in the Ground and Design of Earth Retaining Structures, ASCE.

Shukla, S.J., Gupta, S.K., Sivakugan, N., 2009. Active earth pressure on retaining wall for c–φ soil backfill under seismic loading conditions. Journal of Geotechnical and Geoenvironmental Engineering 135 (5), 690–696.

Sitar, N., Mikola R., Candia, G., 2012. Seismically induced lateral earth pressure on retaining structures and basement walls. In: Proceedings of GSP no. 226, pp. 335–358.

Sokolovskii, V.V., 1965. Statics of Granular Media. Pergamon Press, New York.

Tiznado, J.C., Rodriguez-Roa, F., 2011. Seismic lateral movement prediction for gravity retaining walls on granular soils. Soil Dynamics and Earthquake Engineering 31, 391–400.

Watanabe, K., Koseki, J., Tateyama, M., 2011. Seismic earth pressure exerted on retaining walls under a large seismic load. Soils and Foundations 51 (3), 379–394.

Wood, de V., 1876. The Elements of Analytical Mechanics, John Wiley and Sons, New York. Available from: ⟨books.google.com⟩ (accessed 03.07.11.).